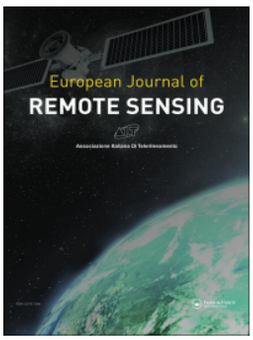

European Journal of Remote Sensing

ISSN: (Print) (Online) Journal homepage: https://www.tandfonline.com/loi/tejr20

Trees outside forest in Italian agroforestry landscapes: detection and mapping using sentinel-2 imagery

Maurizio Sarti, Marco Ciolfi, Marco Lauteri, Pierluigi Paris & Francesca Chiocchini

To cite this article: Maurizio Sarti, Marco Ciolfi, Marco Lauteri, Pierluigi Paris & Francesca Chiocchini (2021) Trees outside forest in Italian agroforestry landscapes: detection and mapping using sentinel-2 imagery, European Journal of Remote Sensing, 54:1, 609-623, DOI: 10.1080/22797254.2021.1986678

To link to this article: https://doi.org/10.1080/22797254.2021.1986678

Published online: 03 Nov 2021.

EUROPEAN JOURNAL OF REMOTE SENSING
2021, VOL. 54, NO. 1, 609–623
https://doi.org/10.1080/22797254.2021.1986678

Taylor & Francis
Taylor & Francis Group

Trees outside forest in Italian agroforestry landscapes: detection and mapping using sentinel-2 imagery

Maurizio Sarti, Marco Ciolfi, Marco Lauteri, Pierluigi Paris and Francesca Chiocchini

National Research Council, Research Institute on Terrestrial Ecosystems, Porano, Italy

ABSTRACT

This study proposes an automated method for distinguishing trees (T) from no-trees (NT) by means of optical data. We make use of an optical approach based on a statistical threshold to detect T areas on visible and near infrared bands. An object-based image classification allows to detect three kinds of tree out of forest (TOF) structures: forest patches (FP), isolated trees (IT), tree hedgerows (THR), distinguished from forest (F). Ground truth validation allows estimating the accuracy of classification.

Four optical bands and six spectral indices are compared detecting images' T areas: B2, B3, B4 and B8 bands, Negative Luminance (NL), Normalized Difference Vegetation index (NDVI), Green NDVI (GNDVI), Blue NDVI (BNDVI), Panchromatic NDVI (PNDVI) and Enhanced Vegetation Index (EVI). NL shows a relatively better capability for TOF detection and classification, with overall accuracy (OA) exceeding 92% and p-value = 10^{-5}. Experiments were conducted on optical data acquired by Sentinel-2 in 2016 over the Alfina highland, central Italy. The tree characteristics were extracted exploiting GNU Octave Image Package. Our results show that this new approach could be extended to the detection and mapping of TOF within large areas of agroforestry landscape.

ARTICLE HISTORY
Received 8 January 2021
Revised 24 September 2021
Accepted 24 September 2021

KEYWORDS
Remote sensing; forest inventories; rural landscapes; biodiversity; ecological network

Introduction

Trees and forests are the two facets of the same resource in human-influenced landscapes; trees may occur in different land uses, such as forest and natural wooded lands, agricultural lands and urban lands and they may grow under three main patterns such as compact blocks, scattered in the landscape and in linear formation (De Foresta et al., 2013). Trees occurring on agricultural and grazed lands, along roads or waterbodies and in residential and urban settings are examples of "Trees on land not defined as forest and other wooded land" according to the FAO definition (FAO, 2001).Small woods, tree hedgerows, scattered and isolated trees, also known as Trees Outside Forest (TOF), are key features of rural, cultural but also urban landscapes (Bellefontaine et al., 2002). Although TOF do not cover large areas of rural landscapes, they contribute to the ecological connectivity and functioning of the landscape at different spatial scales, providing environmental and economic benefits (Bellefontaine et al., 2002; Zomer et al., 2016). TOF enrich the soil, promoting plant, animal diversity and structural complexity at a local scale (Manning et al., 2006); they contribute to the protection of soils against wind and water runoff (Merot et al., 1999); they also increase animals' habitat and genetic connectivity of the species at the landscape scale, playing a key role in the maintenance of biodiversity (Baudry et al., 2000; Burel et al., 1998; Saunders et al., 1991). TOF, besides contributing significantly to national biomass and carbon stocks (Schnell et al., 2015a), provide a variety of products and essential environmental services for people in many regions of the world, some of which are independent of land use while others are land-use specific (De Foresta et al., 2013; Shibu, 2009). For example, in agroforestry landscapes where TOF coexist with agricultural land or pastures, tree hedgerows along fields' borders can be managed as living fences and also used as firewood, improving farmstead energy efficiency as well as carbon sequestration. Fruit trees, other than raising the farmers' income, provide shade for livestock (De Foresta et al., 2013). Moreover, for some communities, the aesthetical and cultural values of TOF might be more important while, for others, the provision of food, firewood, fodder and income might prevail (Schnell et al., 2015a).

The interest in TOF has been growing in recent decades in many countries (Malkoç et al., 2021; Mosquera-Losada et al., 2018; Rigueiro-Rodríguez et al., 2009). In Europe, for example, the European Commission promotes TOF within the agro-environmental measures of the Common Agriculture Policy (CAP) (Santiago-Freijane et al., 2018). Notwithstanding the debated effectiveness of these measures, they should encourage sustainable land use practices along with the preservation of the environment and the countryside.

CONTACT Marco Ciolfi marco.ciolfi@cnr.it National Research Council, Research Institute on Terrestrial Ecosystems, Via Marconi 2, Porano 05010, Italy

The importance of TOF is widely recognized and several studies have been published over the last years, as detailed in the following. However, data on TOF are still scarce and the available information is fragmented at regional and national level. The monitoring and assessment of TOF vary across different countries as reviewed by Schnell et al. (2015b). According to these authors, the combination of field surveys and remote sensing is a suitable approach for improving TOF estimates. Beckschäfer et al. (2017) give an overview of inventory approaches suitable for the assessment of TOF, specifically on agricultural lands. Many studies used remotely sensed data in order to make a global assessment of TOF. Since recognition of TOF over a wide spatial extent is time-consuming if based on visual interpretation only, several studies implemented automatic processes for detecting TOF. Usually, a first phase of study consists in mapping and separating forest vegetation from non-forest vegetation; in a second phase, different kinds of TOF are classified according to their geometrical properties. Meneguzzo et al. (2013) compared pixel- and object-based classification approaches in mapping trees outside forest using high-resolution aerial imagery. An object-oriented classification of very high-resolution airborne imagery was proposed by Tansey et al. (2009) for the extraction of hedgerows in agricultural areas. Recently, Bolyn et al. (2019) proposed a sophisticated classification method of TOF in order to support the operational management of TOF in rural landscape. Particularly, they used open-source software tools, orthophoto and LIDAR-based canopy height model. Other authors used high-resolution satellite imagery, as Singh and Chand (2012). They proposed a combined approach of remote sensing and GIS based spatial technique, integrated with field data for mapping TOF and estimating their biomass. Vannier and Hubert-Moy (2014) evaluated and compared various optical remote sensing data, including high and very high spatial resolution, active and passive sensors and airborne and satellite data. They further adopted an object-based image analysis for detecting and mapping linear elements, such as hedgerows in complex landscapes. A very recent study by Malkoç et al. (2021) proposed an automated approach for mapping TOF at the countrywide scale for Switzerland, based on a high-resolution Vegetation Height Model. However, the proposed method can be repeated for other countries, provided a VHM is available. In the last few years, the launch of the Sentinel-2 satellite has made available data with high spatial and temporal resolution, particularly suitable for the detection of vegetation. Sentinel-2 products are also openly accessible and freely available for all the continental land surfaces of the world, making it easy to integrate such imagery in forest mapping. Recently, Ottosen et al. (2020) used Sentinel-2 images for producing tree cover maps across Europe, achieving results with high thematic accuracy. Brandt and Stolle (2021) developed a deep learning model to classify TOF across large and heterogeneous landscapes of the globe, basing on the use of fused multi-temporal imagery from Sentinel-1 and Sentinel-2.

Traditional tree-based agriculture systems are widespread in Italy, as well as in other Mediterranean countries, involving different multipurpose trees, such as chestnut (*Castanea sativa*), oaks (*Quercus* spp.), and olive trees (*Olea europaea*), (Eichhorn et al., 2006; Paris et al., 2019; Rigueiro-Rodríguez et al., 2009). However, a quantitative estimation of these systems, both at regional and national level, is not actually known.

In this study, we propose an automated method to distinguish between tree (T) and not tree (NT) land cover and to map TOF in an Italian agroforestry landscape, using the freely available Sentinel-2 Multispectral Instrument (MSI) data. We adopted an optical approach consisting in: 1) an automatic identification of tree covered surface, by applying a statistical threshold on visible and near infrared bands; 2) an object-based image analysis to classify TOF elements in three categories, i.e. isolated trees (IT), tree hedgerows (THR) and little groves or forest patches (FP), these elements are separated from forest ones (F); 3) a ground truth validation process.

The procedure has been developed and tested in two Areas of Interest (AoI), both involving Sentinel-2 Multispectral Instrument (MSI) data, considering: 1) four MSI bands (B2, B3, B4 and B8) or 2) a selection of six spectral indices. These latter are Negative Luminance (NL), Normalized Difference Vegetation Index (NDVI), Green and Blue Normalized Difference Vegetation Indices (GNDVI and BNDVI), Panchromatic Normalized Difference Vegetation Index (PNDVI) and Enhanced Vegetation Index (EVI). Based on the best performing index for the two AoI, we finally derived a classification of the full Sentinel-2 subset area.

Materials and methods

Study area

The study area is located in the municipality of Castel Giorgio in Umbria Region (central Italy), on the Alfina highland , a component of the Vulsinian volcanic area standing northeast of Bolsena Lake (figure 1). It is a rural area with high incidence of agroforestry surface. The average elevation is around 500 m, the annual mean temperature is 13°C and the annual mean precipitation is 706 mm.

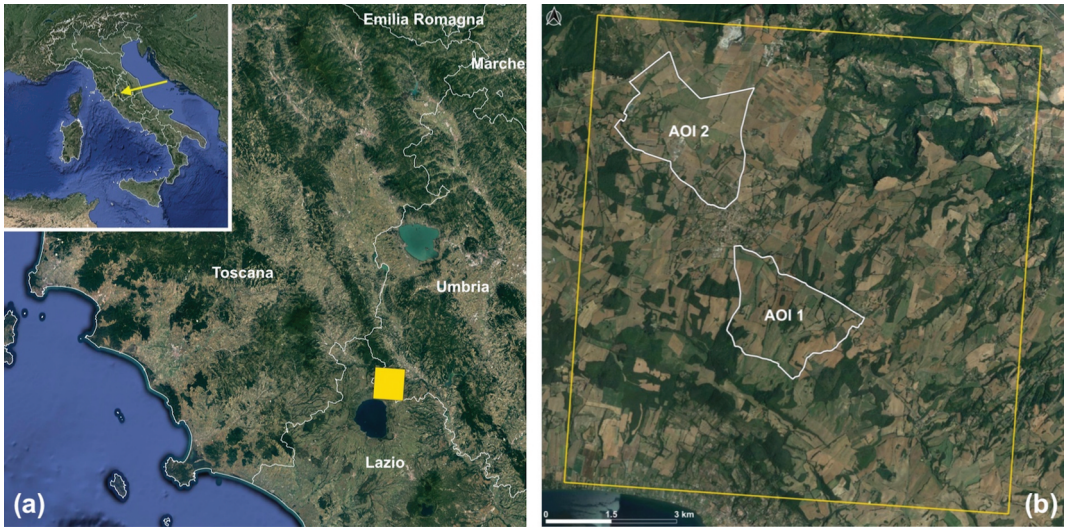

Figure 1. (a) Location of Castel Giorgio municipality, Alfina highland , central Italy; the yellow square corresponds to the Sentinel-2 subset; (b) detail of the two areas of interest (white polygons) and the Sentinel-2 subset (yellow). Images superimposed on GoogleEarth™ satellite base.

A mixed matrix of both agriculture and forestry land uses characterises the landscape, resulting in a mosaic of fragmented patches of different sizes for both land uses. In this way, main landscape elements include crops (mostly wheat, barley, sunflower, rapeseed, pulses, clover and alfalfa), tree hedgerows, shelterbelts and forest areas (with prevalence of broad-leaved trees, mainly *Quercus* spp). Aside the extended forest patches, trees grow at the edges of the fields, within hedgerows, or on scarps and drainage ditches between the fields, as isolated trees or little groves. In such a diversified context and following the criterion of an abundant TOF occurrence, we selected two AoI for testing the automated procedure as shown in figure 1b.

Satellite imagery collection and pre-processing

In the present study, we used Sentinel-2 images (level-1C product; tile number T32TQN), downloaded from the Copernicus Open Access Hub (ESA, 2018a) (https://scihub.copernicus.eu/). We selected a subset of imagery for the year 2016, basing on the vegetative season, as reported in Table 1.

The images have been chosen taking care of absent or minimal cloud/haze (<10%). Furthermore, their chronology catches different plant phenological stages (e.g., recently renewed crown foliage, mature and senescent foliage), and ecophysiology responses to the variable spring, summer and fall conditions (e.g., photosynthesis, transpiration). Finally, the same images contain TOF elements with different aggregated crowns patterns.

Three level-1C Sentinel-2 images, covering the study area, were pre-processed using the Sentinel Application Platform (SNAP) version 5.0.0 (ESA, 2018b). The ESA Sen2Cor processor, version 2.4.0, was used to perform atmospheric and terrain correction of Top-Of-Atmosphere (TOA) Level-1C input data, creating Level-2A Bottom-Of-Atmosphere reflectance (BOA) images (ESA, 2018c). Optical images were also terrain-corrected using a 30 m resolution Shuttle Radar Topography Mission (SRTM) digital elevation model (Farr et al., 2007) and re-projected to UTM WGS84, Zone 32. A spatial sub-setting was performed to constrain the analysis to a geographic area spanning 1077 × 1391 pixels. The B2, B3, B4, and B8 bands, in each of the three scenes, were imported to GNU Octave, version 4.0.0 (Eaton et al., 2015) for the processing step.

Ground truth data

Google Earth very high-resolution images were used to visually identify and classify TOF in the two AoI (IT as point features, THR as line features and FP as polygons) and to produce a ground truth map. Moreover, single trees and aligned trees have been georeferenced on site using a Garmin Montana GPS.

Processing method overview

Several previous studies (Colwell, 1974; Goward et al., 1994; Huemmrich & Goward, 1997) showed that the forest is generally darker than most other vegetated surfaces in the visible and shortwave infrared bands and is among the most easily identifiable feature in remote sensing imagery (Dodge & Bryant, 1976). The spectral response of deciduous trees is low in the visible and shortwave infrared bands and it is high in near infrared band, as it is the case in our agroforestry landscape, without coniferous TOF.

Table 1. List of Sentinel-2 images used in this study.

N	Identifier data	Acquisition date
1	S2A_MSIL1C_20160628T101032_N0204_R022_T32TQN_20160628T101826	28/06/2016
2	S2A_MSIL1C_20160718T101032_N0204_R022_T32TQN_20160718T101028	18/07/2016
3	S2A_MSIL1C_20160926T101022_N0204_R022_T32TQN_20160926T101754	26/09/2016

We used an optical approach based on a statistical threshold to detect T pixels on visible and near infrared bands. An object-based image analysis was then applied to distinguish the three kinds of TOF elements. In this way, isolated trees (IT), tree hedgerows (THR) and forest patches or groves (FP), were detected and classified using a decision process.

In detail, we consider four MSI bands: B2 (blue, 490 nm), B3 (green, 560 nm), B4 (red, 665 nm) and B8 (near infrared, 842 nm) and we evaluated a selection of spectral indices and bands combination: NDVI, GNDVI, BNDVI, PNDVI, EVI, and NL, as reported in Table 2. We used the visible bands, reversing their sign (–B2, –B3 and –B4) instead of their original values for homogeneity with the vegetation indices and the near infrared (B8) histograms, so that the tree pixels fall in the rightmost histogram peak (Table 2). Afterwards, we performed an image fusion of the three images over time, through minimization of each spectral index and band combination. This procedure highlights trees from crops and other time-varying coverages in the resulting fused image. Basing on such assumption, we used the time-minimized images to detect T areas, obtaining trees pixels (isolated, grouped or belonging to a forest) in the rightmost peak of their image histogram. Finally, we compared the respective resulting tree maps with ground truth. A flow chart of the classification workflow of this study is shown in Figure 2.

Tree pixels identification

The identification of T pixels was performed on local image windows, containing the two AoI, by identifying the forest peak values and then thresholding the time-minimized images. We assumed that the T peak coincides with the rightmost peak in the distribution of pixels $D(x)$ in the image histogram.

According to Scott (1979) the optimal histogram bin width (h_n) is assumed as:

$$h_n = 3.49sn^{-1/3}$$

where $s = 1.4826\ mad(x)$ is the estimation of standard deviation derived from the mean absolute deviation without outliers (*mad*) of the distribution and n is the sample size.

The automatic identification of T pixels is achieved according to the following rules:

x is T if $D(x) \geq t$

x is NT if $D(x) < t$

where t is the threshold value identified by the forest peak in the image histogram.

Assuming the T distribution to be Gaussian ensures that the mean (μ), the median and the mode coincide, and that the width can be taken as the standard deviation σ. The distribution parameters are estimated from the histogram, in particular, μ is taken as the mode of the T pixels' peak (the rightmost one) and σ is estimated from the upper-half distribution of T (the shaded area in figure 3):

$$\sigma = \sqrt{\frac{1}{N}\sum_{x_i > \mu}(x_i - \mu)^2}$$

where N is the number of pixels greater than μ. As the threshold value, we take:

$$t = m - z\sigma$$

where z is the standard normal distribution z-value (Table 3).

Figure 3 shows an example of the index distribution for two synthetic populations where the overlap of two tiles increases the relative frequency in real distribution (e.g., NDVI for T and NT with index μ equal to 0.7 and 0.4, and σ equal to 0.5 and 0.1, respectively).

Object-based image analysis and classification

Following an object-based analysis in order to achieve a real-world interpretation of the images, pixels are grouped into segments, which form the minimum classification unit. The segments are classified on the basis of both T maps and hierarchical approach, by using the spectral, textural and spatial attributes of the single segments.

The objects in a given digital pattern are segments of the T maps. In our classification we assumed 20 × 20 m (i.e. 2 × 2 pixels) as the largest area covered by an isolated tree.

The T maps (binary images [0,1]) were processed in GNU Octave (Eaton et al., 2015). The *bwboundaries* and *regionprops* functions of the GNU Octave Image Package allowed us to identify all the external boundaries of the objects in the T maps. Once the T object structures were singled out, we evaluated their geometrical properties such as the area, perimeter, eccentricity, rectangularity, etc. The objects were classified according to four classes in the decision tree, IT, THR, FP and F via the following rules:

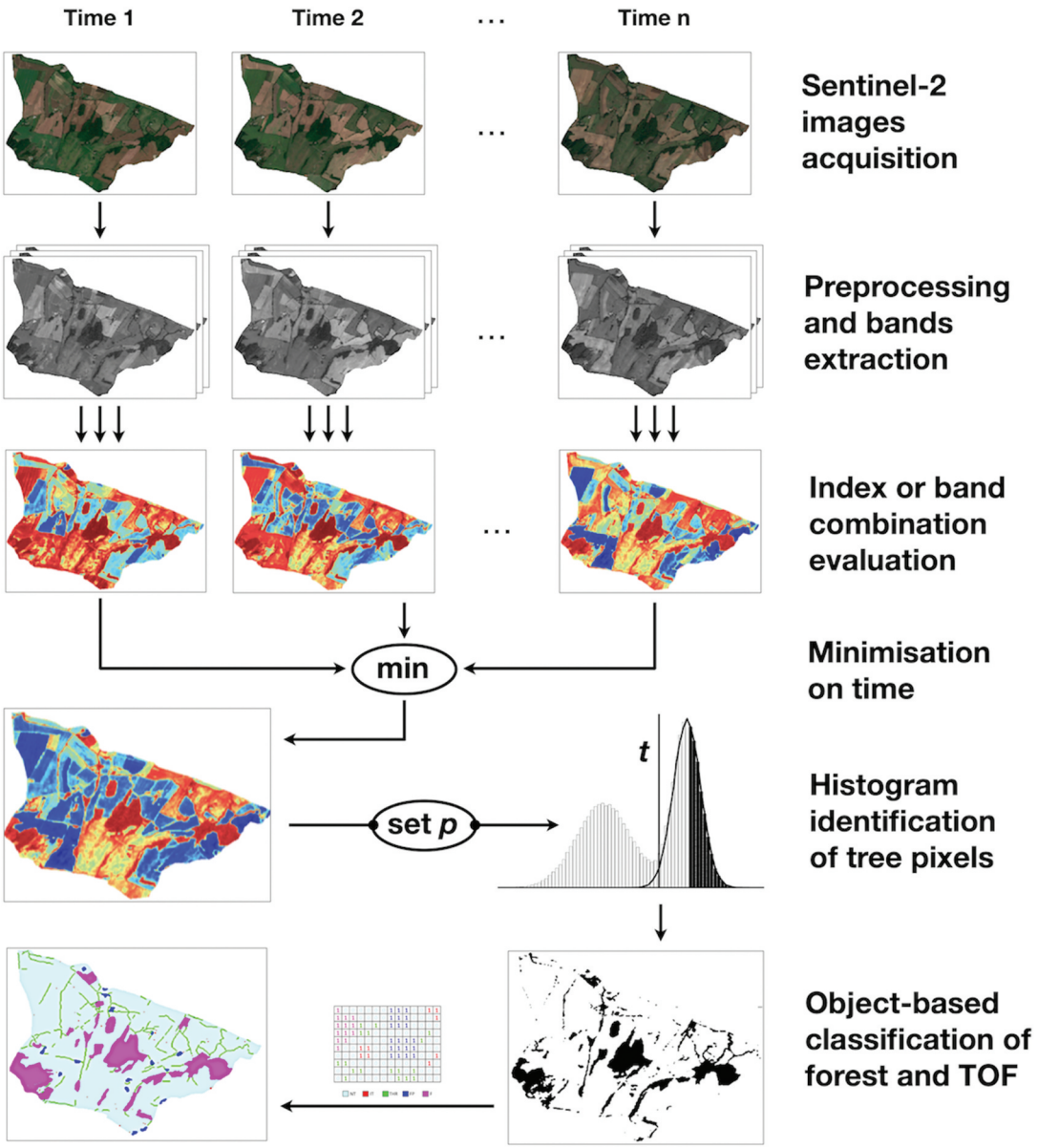

Figure 2. Flow chart of the classification workflow.

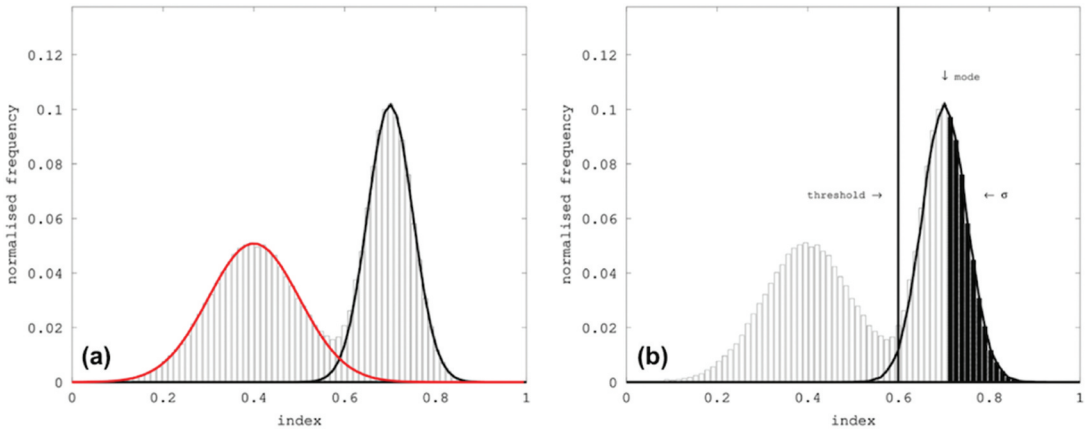

Figure 3. (a) Distribution of two synthetic populations (red and black curves) with index mean 0.4 (left) and 0.7 (right), standard deviation 0.1 (left) and 0.05 (right); (b) Estimate of the μ and σ parameters of the last peak of the histogram. μ is the mode of last peak and σ is taken as the half-width of the last histogram peak. The threshold t corresponds to a p-value 0.05 in the left peak tail.

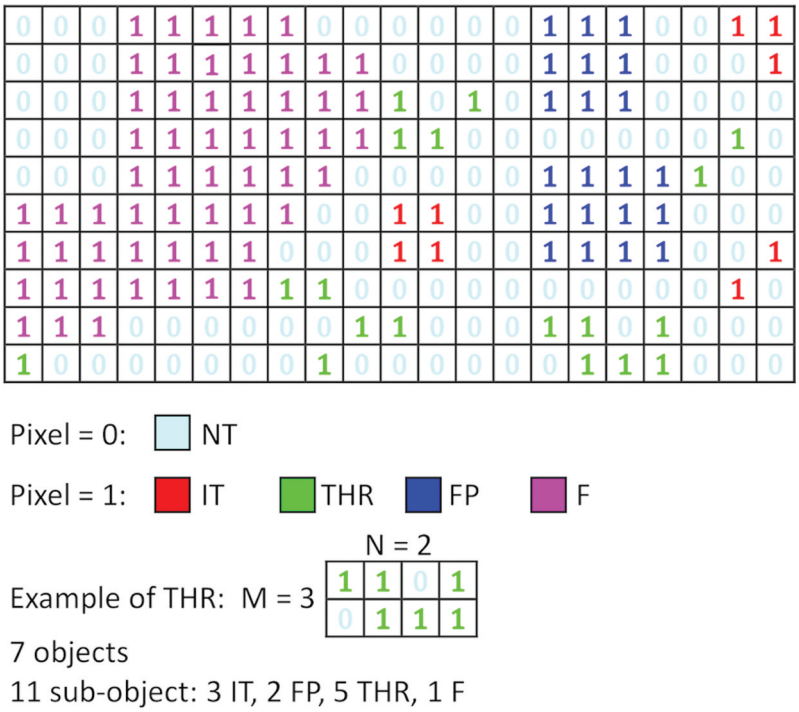

Figure 4. An example of objects classification in tree (T) and not tree (NT) map [1,0] according with four types of tree structures: isolated tree (IT), tree hedgerow (THR), forest patches (FP) and forest (F).

- IT: if max (N,M) <3 (small, nearly circular, structures);
- THR: if max (N,M) >2 and not all pixels of every 3 × 3 sub-structure within the object are 1 (elongated structures, without a limiting length);
- FP: if all the pixels of 3 × 3 sub-structures within the object are 1 and total pixels are < 50 (relatively large uniform patches, still with a small extent);
- F: if all pixels of 3 × 3 sub-structures within the object are 1 and total pixels identified are ≥50 (the larger uniform patches);

where M and N are the number of pixel equal to 1 on the principal and the perpendicular object axis (or sub-structure within the object).

Figure 4 shows an example of objects classification in T and NT, according with four types of tree structures.

Ground truth identification of TOF and classification accuracy assessment

Recognition of TOF was also performed, in QGIS environment (QGIS, 2018), by visual photo interpretation of high-resolution imagery from Google Earth, for both AoI 1 and 2. Single trees (IT) and aligned trees, such as THR, were georeferenced on site with a Garmin Montana GPS device as additional ground truth reference data. IT, THR FP and F were digitized and represented respectively as point, line and polygon features in QGIS. Then, point and line features were buffered (with a buffer distance of 10 m, according with images spatial resolution) to obtained polygon representations of the trees' crowns coverage for IT and THR. Afterwards TOF vector features were converted to raster data for the validation of automatically detected TOF maps.

We used confusion matrix (or error matrix) method to assess the accuracy of the image classification results. The error matrix compares, on a class-by-class basis, the relationship between known reference data (ground truth) and the corresponding results of the classification procedure. We use the results of TOF identification based on visual interpretation of Google Earth images and GPS georeferencing as reference data for the computation of confusion matrix.

According to Congalton (1991), we evaluated the Overall Accuracy (OA) as accuracy metric. The OA is computed by dividing the total number of correctly classified pixels (i.e., the sum of the elements along the principal diagonal) by the total number of reference pixels. We also calculated the Producer Accuracy (PA), representing how accurately the reference pixels of the ground cover type are classified, and the User Accuracy (UA), representing the probability that a pixel classified into a given category actually represents that category on the ground. These metrics were calculated for all the resulting T maps relative to the two AoI, for each of the optical bands and the spectral indices, seeking for the best match.

Table 2. Sentinel-2 MSI bands, band combination and indices considered in the study: – B2 (Negative Blue), – B3 (Negative Green), – B4 (Negative Red) and B8 (Near Infrared), NL (Negative Luminance), Normalized Difference Vegetation Index (NDVI), Green and Blue Normalized Difference Vegetation Indices (GNDVI and BNDVI), Panchromatic Normalized Difference Vegetation Index (PNDVI) and Enhanced Vegetation Index (EVI).

Index	Name	Sentinel-2 MSI band combination	Reference
NB	Negative Blue	-B2	
NG	Negative Green	-B3	
NR	Negative Red	-B4	
NIR	Near Infrared	B8	
NL	Negative Luminance	$-(0.299B4 + 0.587B3 + 0.114B2)$	J Yang et al. (2010)
NDVI	Normalized Vegetation Index	$B8 - B4/B8 + B4$	Rouse et al. (1973)
GNDVI	Green Normalized Vegetation Index	$B8 - B3/B8 + B3$	Gitelson (1996)
BNDVI	Blue Normalized Vegetation Index	$B8 - B2/B8 + B2$	C Yang et al. (2004)
PNDVI	Panchromatic NDVI	$B8 - (B4 + B3 + B2)/B8 + (B4 + B3 + B2)$	Wang et al. (2007)
EVI	Enhanced Vegetation Index	$GB8 - B4/B8 + C1B4 - C2B2 + L$ with G = 2.5, C1 = 6, C2 = 7.5, and L = 1	Huete et al. (1999)

Basing on the best performer index, we finally classified T pixels over the full Sentinel-2 subset area, identifying objects as IT, THR, FP and F.

Results and discussion

Tree pixels identification

Natural colour RGB composition of Sentinel-2 images for the two AoI and for three dates of acquisition (see Table 1) are shown in Figure 5.

Some parts of the observed scenes are time-invariant while others change over time. The time-invariant units of the images correspond to potential T pixels, while the time-varying units are all considered as NT (e.g., crops, meadows).

Figure 6 and 7 show for AoI 1 and AoI 2, respectively, the maximum value for natural colour imagery (RGB composition) (a), the minimum value of NB (b), NG (c), NR (d), NIR bands (e), and NL (f). Figures 6 and 7 highlight a clearer separation of T (orange-red colour) from NT (blue-cyan colour).

For the identification of T pixels we evaluated five thresholds to separate T from NT pixels, generating five T maps for each index.

The confusion matrix was calculated using ground truth data for estimating the image classification accuracy. The quantitative results for the identification of T pixels with our proposed method are summarized in Table 4, concerning either AoI 1 and AoI 2. Table 4 shows the OA (%) evaluated for five significance p-values from 10^{-2} to 10^{-6}, for each band and spectral index; an asterisk (*) marks the two best comparison results for each given p-value for each AoI.

Table 3. Significance level p-value and z for lower tailed test.

p	z
$\mathbf{10^{-2}}$	2.326
$\mathbf{10^{-3}}$	3.090
$\mathbf{10^{-4}}$	3.719
$\mathbf{10^{-5}}$	4.264
$\mathbf{10^{-6}}$	4.753

The best performance is given by the NL with nine total asterisks for the OA (Table 4). Notice that NG gives the best performance by yielding five asterisks both for the OA for the AoI 1, but none for the AoI 2. The NIR shows the worst detection scores. In fact, the T pixels are completely overlapped with the NT pixels in histogram of NIR (data not shown). All tested indices based on NIR (BNDVI, GNDVI, PNDVI and EVI) also showed a weak capability in separating T from NT pixels. In both the AoI, the NT pixels mainly correspond to agricultural vegetation, with herbaceous land cover during the reference periods. This evidence would explain the low discriminating power between T/NT cover of the vegetation indices in rural areas. The balanced linear combination of NB, NG and NR makes NL the best index for the T/NT discrimination. For all the given p-values, the performances of NL are similar for the OA for both AoI 1 and 2.

Figure 8a shows the index distribution for NL with p-value = 10^{-5} and the identification of T populations for both AoI 1 (b) and AoI 2 (c).

Sentinel-2 images allowed mapping tree cover with high accuracy as confirmed in a recent study by Ottosen et al. (2020), which produced tree maps from Sentinel-2, with high thematic accuracy, for several European areas, showing that the imagery resolution allows the identification of TOF.

Object-based image classification of TOF and accuracy assessment

The object-based classified TOF map and the ground truth TOF data for AoI 1 and 2 are used as the input for the computation of the confusion matrices (Tables 5 and Tables 6, figure 9).

Table 5 and Table 6 show the confusion matrices, respectively for AoI 1 and 2, and the accuracy metrics for the TOF classification based on NL, with

Table 4. The Overall Accuracy (%) for AoI 1 and 2, with significance level *p*-values from 10^{-2} to 10^{-6}, for bands, bands combinations and indices are compared to detect T areas: Negative Blue (NB), Negative Green (NG), Negative Red (NG), Near Infrared (NIR), Negative Luminance (NL), Normalized Difference Vegetation Index (NDVI), Green Normalized Difference Vegetation Index (GNDVI), Blue Normalized Difference Vegetation Index (BNDVI), Panchromatic NDVI (PNDVI) and Enhancement Vegetation Index (EVI). The last column shows the number of best performing variables.

	Area 1					Area 2					Best count
p	10^{-2}	10^{-3}	10^{-4}	10^{-5}	10^{-6}	10^{-2}	10^{-3}	10^{-4}	10^{-5}	10^{-6}	N
NB	92.90*	93.33	93.40	93.31	93.05	93.46*	93.67*	93.69*	93.63	93.49	1 + 3
NG	93.08*	93.69*	93.85*	93.83*	93.55*	93.18	93.37	93.22	92.85	92.20	5 + 0
NR	92.33	92.56	92.61	92.50	92.25	93.36	93.55	93.68	93.76*	93.76*	0 + 2
NIR	61.32	45.26	33.06	33.06	33.06	69.42	43.13	32.14	32.14	32.14	0 + 0
NL	92.78	93.34*	93.69*	93.64*	93.60*	93.42*	93.76*	93.73*	93.65*	93.50*	4 + 5
NDVI	91.69	91.71	91.54	91.19	91.19	92.71	93.02	93.27	93.37	93.37	0 + 0
GNDVI	91.98	92.22	92.60	92.64	92.55	92.11	92.38	92.84	93.02	93.16	0 + 0
BNDVI	91.29	91.27	90.97	90.62	90.09	92.35	92.65	92.87	93.01	93.13	0 + 0
PNDVI	91.66	92.09	92.14	91.96	91.60	92.14	92.64	92.85	93.18	93.30	0 + 0
EVI	74.24	70.39	67.96	64.91	60.04	87.67	81.35	71.76	61.33	50.97	0 + 0

Table 5. Confusion matrix and accuracy measures for the Negative Luminance (NL) based classification of T, NT, TOF, with significance level $p = 10^{-5}$ for the AoI 1.

	Reference Data						
	NT	IT	THR	FP	F	Total	UA (%)
Not Tree (NT)	50,150	29	953	199	1304	52,635	95.27
Isolated Tree (IT)	80	8	44	0	4	136	05.88
Tree Hedgerow (THR)	816	4	513	154	374	1861	27.56
Forest Patches (FP)	103	0	36	183	40	362	50.55
Forest (F)	559	0	137	0	7938	8634	91.93
Total	51,708	41	1683	536	9960	63,628	
PA (%)	96.98	19.51	30.48	34.14	82.17		
OA (%)	92.39						

p-value = 10^{-5}. The results are similar for both AoI: OA is 92.39% for AoI 1 and is 92.47% for AoI 2. The best classified class is NT with a Producer Accuracy (PA) at least 96.61% and a User Accuracy (UA) of 95.23% while the worst classification score is for IT, with a smallest PA 11.29% and UA 3.97%. In fact, the classification procedure overestimated the IT class for both AoI, especially with respect to NT and THR classes of the reference map (see Tables 5 and Tables 6). This result may derive from the different spatial resolution between the Sentinel-2 images used for the classification and the Google Earth images used to produce the reference map. Although the Sentinel-2 images have high spatial resolution, the minimum pixel unit of 10 × 10 m may contain spectral information of more than one land cover/use type, which can lead to misclassification.

The numerical results of confusion matrix suggest that NT are always well identified followed by the F class. The IT, THR and FP are no so well identified from the numerical point of view while a visual comparison between automatically classified TOF maps and ground truth TOF maps of AoI 1 and 2 reveals similarity. Indeed, in figure 9 we show the ground truth classification for AoI 1 and 2, based on visual classification by photo interpretation, while in figure 9 the corresponding NL automated classification with $p = 10^{-5}$. Although the patterns of NL classification well describe the observed scenes, there are several mismatches between the numerical and the visual classification results. Such inconsistencies could be attributed to the following reasons: 1) differences in the resolution of satellite data used for the

Table 6. Confusion matrix and accuracy measures for the Negative Luminance (NL) based classification of T, NT, TOF, with significance level $p = 10^{-5}$ for the AoI 2.

	Reference Data						
	NT	IT	THR	FP	F	Total	UA (%)
Not Tree (NT)	65,651	42	1312	80	1143	68,228	96.22
Isolated Tree (IT)	105	7	61	3	0	176	3.97
Tree Hedgerow (THR)	1012	10	599	37	371	2029	29.52
Forest Patches (FP)	141	0	55	23	146	365	6.30
Forest (F)	1043	3	144	76	4789	6055	79.09
Total	67,952	62	2171	219	6449	76,853	
PA (%)	96.61	11.29	27.59	10.50	74.25		
OA (%)	92.47						

classification of reference map (very high-resolution Google Earth images) and automated classification map (high-resolution Sentinel-2 images); 2) spatial shift between the ground truth map and the reconstructed map. This is the case with a misaligned crown with respect to the stem in non-nadiral aerial imagery; 3) the choice of threshold t; for instance, in the discrimination of a THR, some T could be below the threshold t. This could lead to several interruptions along the reconstructed THR, several sub-THR interspersed with IT; 4) possible misclassifications by the human interpreter in the reference map.

According to previous studies by Liknes et al. (2010) and Meneguzzo et al. (2013) an object-based image analysis approach is much better at mimicking how a human interpreter groups trees into patches, and allows for better patch-based metrics for describing spatial pattern, in comparison with a pixel-based approach. Due to the varying nature of the agroforestry landscape, we chose a topological approach to the TOF classification, limiting classes only to points (IT), lines (THR) and surfaces (FP), without introducing any pattern in the TOF spatial arrangement. However, the knowledge of a local pattern could be exploited to improve the spatial accuracy of the classified TOF (Khan et al., 2018). The proposed method, based only on free optical data, allowed us to perform a TOF classification accurate enough to distinguish IT, THR and FP, although coarser than the classification achieved by Bolyn et al. (2019), who exploited orthophoto and LIDAR data. Moreover, the open accessibility of Copernicus Sentinel products for all the continental land surfaces and their short revisit time makes the proposed method easy to replicate over large rural areas. Locally integrating other information sources, e.g., a detailed vegetation height map as in Malkoç et al. (2021) could improve the accuracy of trees identification and TOF classification. Image pre-processing should also include a slope adjustment in case of rugged terrain, as our study area is relatively flat. Suitably detailed Digital Terrain Models are generally available worldwide. Further improvement in TOF detection could be achieved integrating the Sentinel-1 SAR imagery (Brandt & Stolle, 2021).

Finally, Figure 10 shows an object-based classification T map for the full Sentinel-2 subset area by NL, with p-value = 10^{-5}. Numbers of pixel and objects identified by Negative Luminance (NL) based classification of T were reported in Table 7.

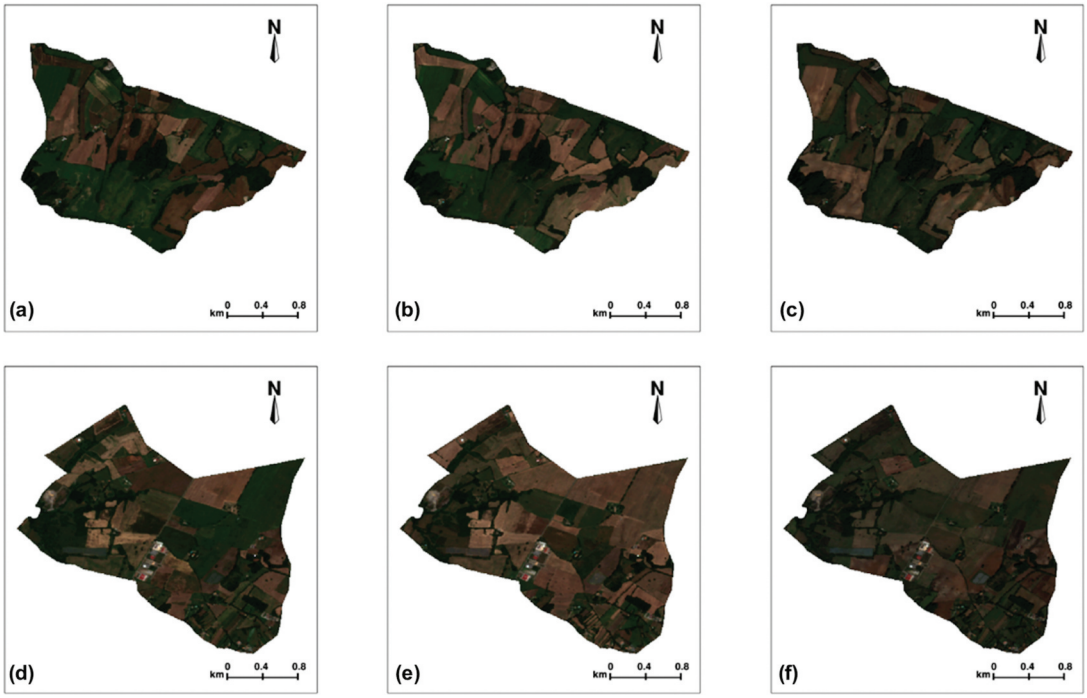

Figure 5. Natural colour Sentinel-2 images for the two areas of interest and for three dates of acquisition. AoI 1: (a) 28 June 2016, (b) 18 July 2016 and (c) 26 September 2016; AoI 2: (d) 28 June 2016, (e) 18 July 2016 and (f) 26 September 2016.

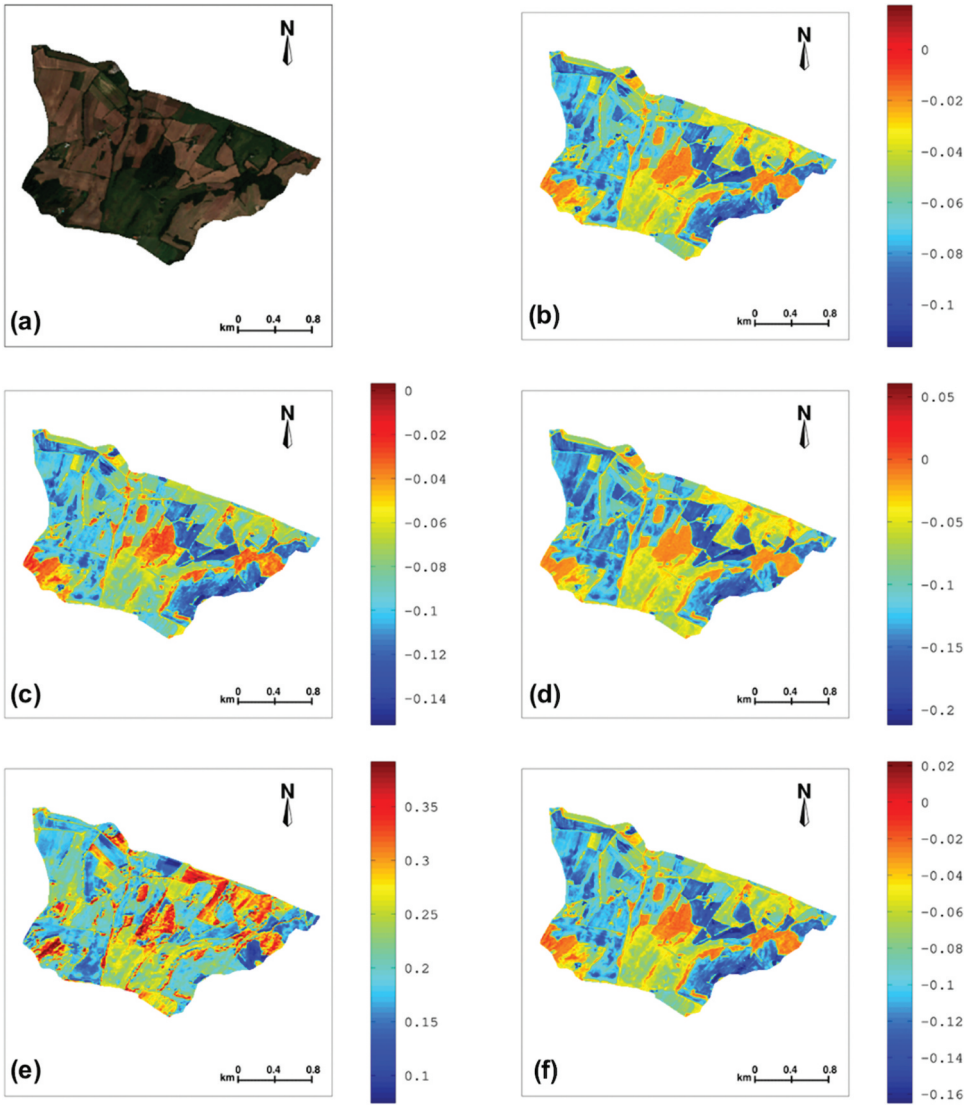

Figure 6. (a) Maximum value for natural colour RGB imagery. Minimum value for: (b) Negative Blue (NB), (c) Negative Green (NG), (d) Negative Red (NR), (e) Near Infrared (NIR), (f) Negative Luminance (NL) for AoI 1.

The availability of cloud computing platforms, like Google™ EarthEngine™ (Gorelick et al., 2017), could speed-up the pre-processing phase (images retrieval, fusion and band extraction), leaving the tree pixels identification and TOF classification for off-grid, local computing.

Conclusions

A procedure for the detection of T/NT land cover and for the automated classification of TOF in rural landscapes, based on optical data, was presented in this study. An optical approach based on a statistical threshold appropriately tailored for visible and near infrared bands was used over Sentinel-2 images in order to automatically identify tree covered surfaces in two areas of interest. The relevance of the single bands B2, B3, B4, B8 and the spectral indices NL, NDVI, GNDVI, BNDVI, PNDVI, EVI was evaluated in the procedure for T identification. NL resulted the best performing spectral index in identifying the tree covered pixels, with the best scores for OA (higher than 93.64%) respect to the other indices. The OA of the automated classification of TOF was about 92% for both area of interest, while the PA and the UA for individual classes resulted low, due to the spatial

Table 7. Number of pixels and objects identified by Negative Luminance (NL) based classification of T, with $p = 10^{-5}$ for the full Sentinel-2 subset area.

	N pixel	N sub-object
Not Tree (NT)	986,493	
Isolated Tree (IT)	2996	1861
Tree Hedgerow (THR)	39,063	1933
Forest Patches (FP)	6572	773
Forest (F)	361,762	195

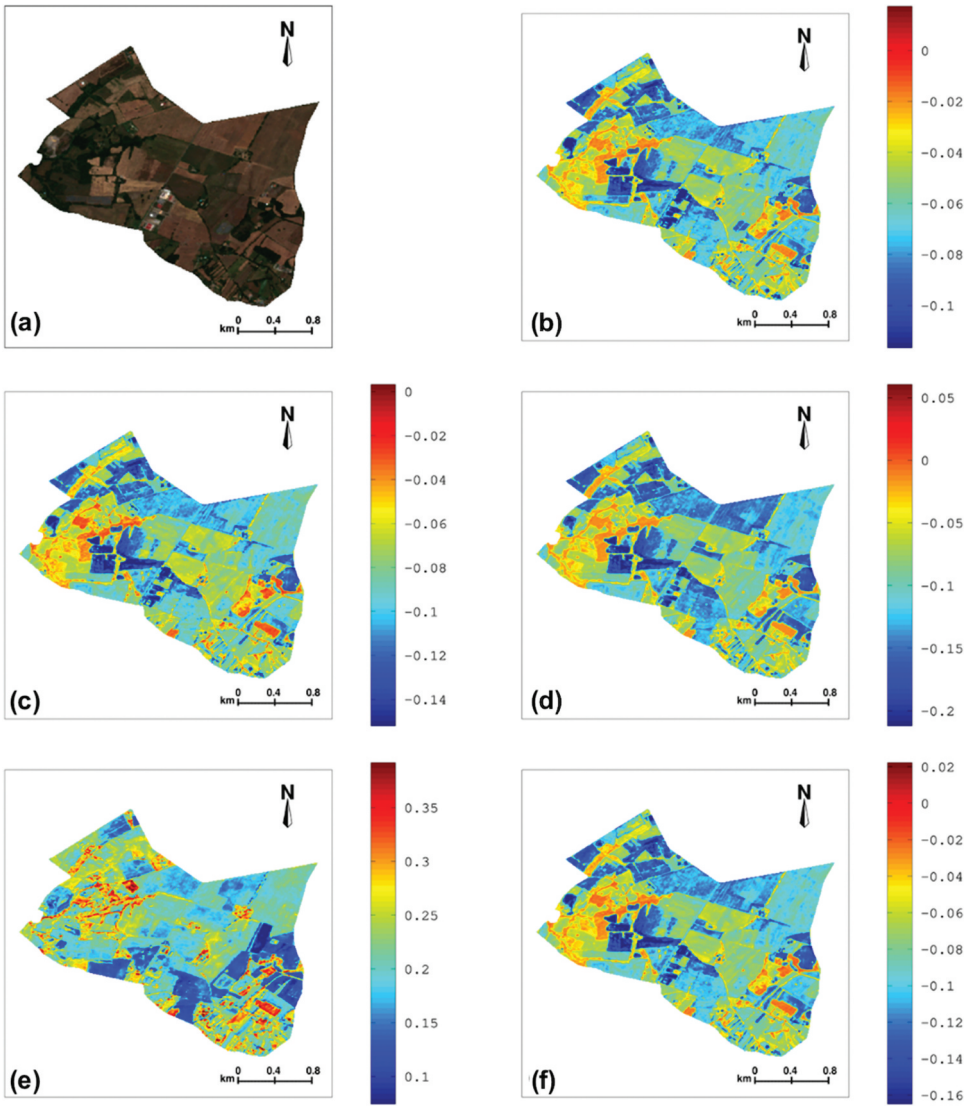

Figure 7. (a) Maximum value for natural colour RGB imagery. Minimum value for: (b) Negative Blue (NB), (c) Negative Green (NG), (d) Negative Red (NR), (e) Near Infrared (NIR), (f) Negative Luminance (NL) for AoI 2.

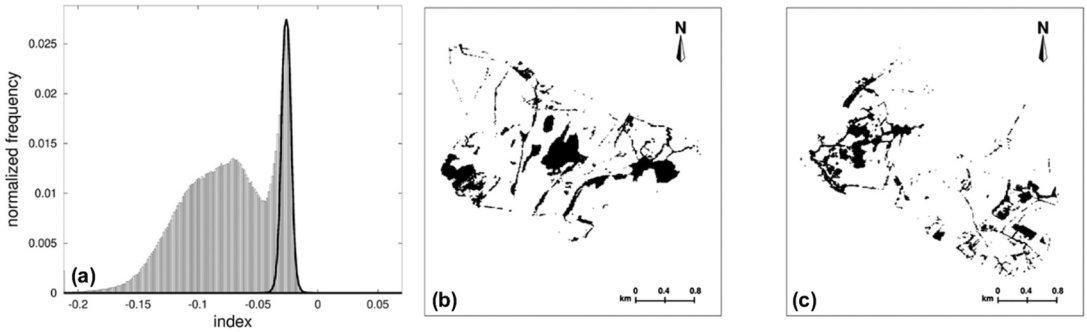

Figure 8. Histogram of Negative Luminance (NL). The tree (T) distribution is identify by the black curve. b) Tree map for area of interest 1 with p-value = 10^{-5}. c) Tree map for area of interest 2 with $p = 10^{-\backslash 5}$.

resolution of Sentinel-2 images. The use of freely available high-resolution Sentinel-2 data set and the use of publicly available software tools allowed us to produce a fairly accurate automated classification of TOF in an Italian agroforestry landscape. The proposed approach is also easily repeatable over large rural areas, thanks to the worldwide coverage of Sentinel-2 images. Such method allowed estimating the TOF covered surface of Italian agroforestry systems, of which little information is available both at

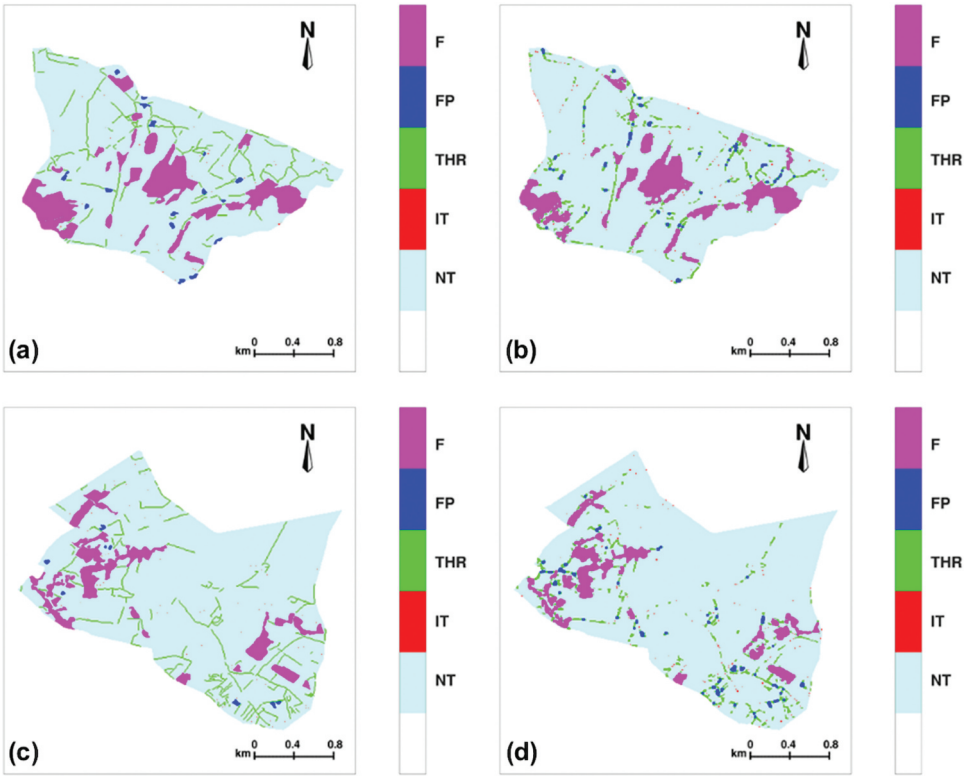

Figure 9. (a) Ground truth classification of area of interest 1. b) Negative Luminance (NL) based classification of area of interest 1 with p-value = 10^{-5}. c) Ground truth classification of area of interest 2. d) NL based classification of area of interest 2 with p= 10^{-5}. The cyan colour stands for No Trees (NT), the red is for Isolated Trees (IT), green for Tree Hedgerows (THR), blue for Forest Patches (FP) and purple for Forest (F).

regional and National scale. Our results also represent

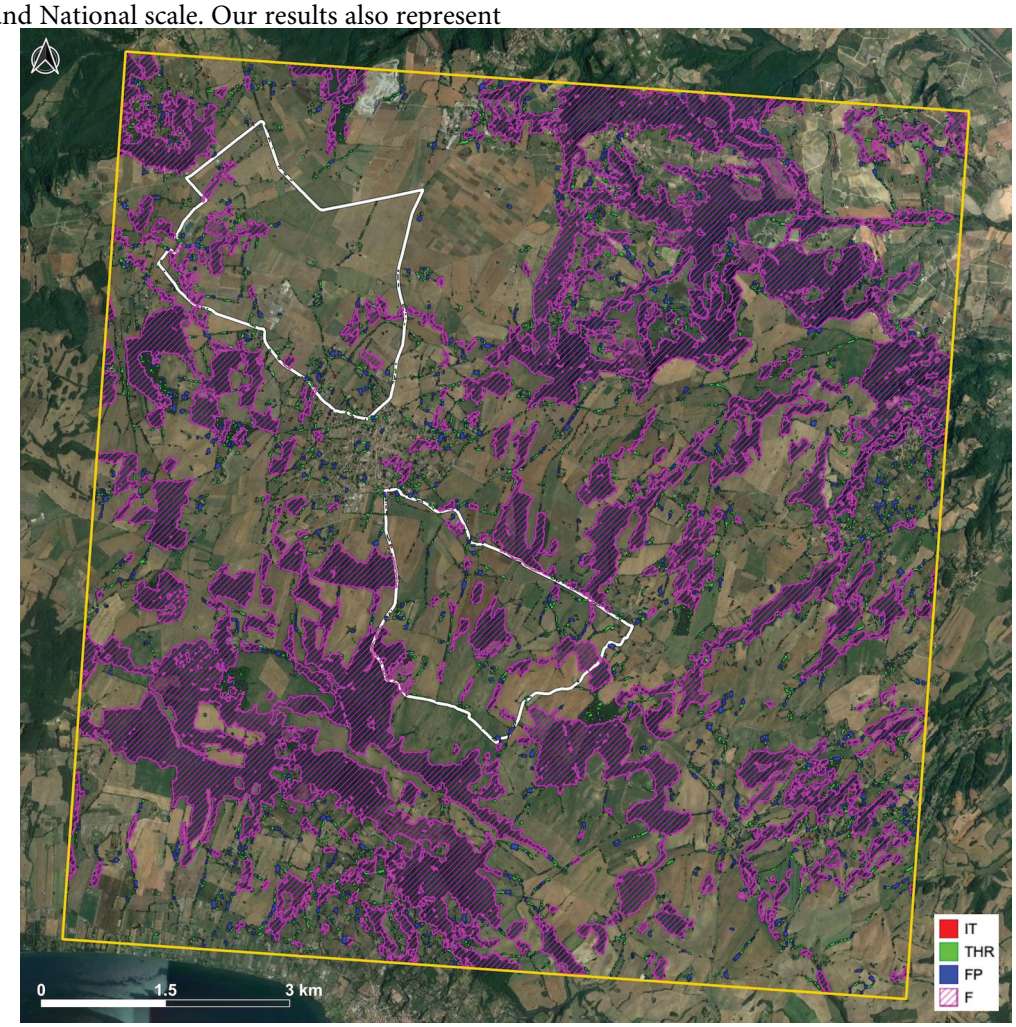

Figure 10. Object-based classification of the full Sentinel-2 subset area: IT = isolated trees, THR = tree hedgerows, FP = forest patches, F = forest. The areas of interest are outlined in white.

new insight in the development of tree mapping algorithms as well as accuracy assessment of such algorithms based on the Sentinel-2 products.

Given likely significant contribution of TOF to national biomass and carbon stocks and provision for essential ecosystem services, filling the lack of information on TOF extension can be crucial to prepare effective agro-environmental measures and rural development policies.

Acknowledgments

This research was developed during the SidaTim project, co-founded by the European Union's Horizon 2020 research and innovation programme under grant agreement N° 652615 (FACCE-JPI). Funding was provided to CNR IRET by national agency (see https://www.sidatim.eu/en/).

Disclosure statement

The authors declare no relevant competing interests.

ORCID

Maurizio Sarti http://orcid.org/0000-0002-5063-4154
Marco Ciolfi http://orcid.org/0000-0003-4831-8053
Marco Lauteri http://orcid.org/0000-0003-1071-7999
Pierluigi Paris http://orcid.org/0000-0003-4822-9392
Francesca Chiocchini http://orcid.org/0000-0002-5122-8756

Data Availability Statement

The data that support the findings of this study are openly available at https://doi.org/10.5281/zenodo.4395832

References

Baudry, J., Bunce, R. G. H., & Burel, F. (2000). Hedgerows: An international perspective on their origin, function and management. *Journal of Environmental Management*, *60*(1), 7–22. https://doi.org/10.1006/jema.2000.0358

Beckschäfer, P., Schnell, S., & Kleinn, C. (2017). Monitoring and assessment of Trees Outside Forests (TOF). In J. C. Dagar & V.P. Tewari (Eds.), *Agroforestry* (pp. 137–161). Springer Nature Singapore Pte Ltd. https://doi.org/10.1007/978-981-10-7650-3_5

Bellefontaine, R., Petit, S., Pain-Orcet, M., Deleporte, P., & Bertault, J. G. (2002). *Trees outside forests. Towards better awareness*. FAO Conservation Guide 35.

Bolyn, C., Lejeune, P., Michez, A., & Latte, N. (2019). Automated classification of trees outside forest for supporting operational management in rural landscapes. Remote Sensing, 11(10), 1146. https://doi.org/10.3390/rs11101146

Brandt, J., & Stolle, F. (2021). A global method to identify trees outside of closed-canopy forests with medium-resolution satellite imagery. *International Journal of Remote Sensing*, *42*(5), 1713–1737. https://doi.org/10.1080/01431161.2020.1841324

Burel, F., Baudry, J., Butet, A., Clergeau, P., Delettre, Y., Le Coeur, D., Dubs, F., Morvan, N., Paillat, G., Petit, S., Thenail, C., Brunel, E., & Lefeuvre, J.-C. (1998). Comparative biodiversity along a gradient of agricultural landscapes. *Acta Oecologica*, *19*(1), 47–60. https://doi.org/10.1016/S1146-609X(98)80007-6

Colwell, J. E. (1974). Vegetation canopy reflectance. *Remote Sensing of Environment*, *3*(3), 174–183. https://doi.org/10.1016/0034-4257(74)90003-0

Congalton, R. G. (1991). A review of assessing the accuracy of classifications of remotely sensed data. *Remote Sensing of Environment*, *37*(1), 35–46. https://doi.org/10.1016/0034-4257(91)90048-B

de Foresta, H., Somarriba, E., Temu, A., Boulanger, D., Feuilly, H., & Gaulthier, M. (2013). Towards the assessment of trees outside of forests. resources assessment working paper. 183 FAO Rome.

Dodge, A., & Bryant, E. (1976). Forest type mapping with satellite data. Journal of Forestry, 74(8), 23–40. https://doi.org/10.1093/jof/74.8.526

Eaton, J. W., Bateman, D., Hauberg, S., & Wehbring, R. (2015). *GNU Octave version 4.0.0 manual: A high-level interactive language for numerical computations. fourth*. Create Space Independent Publishing Platform. URL: http://www.gnu.org/software/octave/doc/interpreter

Eichhorn, M. P., Paris, P., Herzog, F., Incoll, L. K., Mayus, M., Moreno, G., Papanastasis, V. P., Pilbeam, D. J., Pisanelli, A., Dupraz, C., Pisanelli, A., & Dupraz, C. (2006). Silvoarable systems in Europe – past, present and future prospects. *Agroforest Systems*, *67*(1), 29–50. https://doi.org/10.1007/s10457-005-1111-7

European Space Agency (2018a). *Sentinel scientific hub*. URL: https://scihub.copernicus.eu/dhus/#/home (Retrieved January 2020).

European Space Agency (2018b). *Sentinel application platform*. URL: http://step.esa.int/main/toolboxes/snap/ (Retrieved January 2020).

European Space Agency (2018c). *Sen2Cor*. URL: http://step.esa.int/main/third-party-plugins-2/sen2cor/ (Retrieved January 2020).

FAO (2001). Global forest resources assessment 2000 Main report. Food and Agriculture Organization of the United Nations, Rome (2001) - ISSN 0258–6150

Farr, T. G., Rosen, P. A., Caro, E., Crippen, R., Duren, R., Hensley, S., Kobrick, M., Paller, M., Rodriguez, E., Roth, L., Seal, D., Shaffer, S., Shimada, J., Umland, J., Werner, M., Oskin, M., Burbank, D., & Alsdorf, D. (2007). The shuttle radar topography mission. *Reviews of Geophysics*, *45*(2), RG2004. https://doi.org/10.1029/2005RG000183

Gitelson, A. A., Kaufman, Y. J., & Merzlyak, M. N. (1996). Use of a green channel in remote sensing of global vegetation from EOS-MODIS. *Remote Sensing of Environment*, *58*(3), 289–298. https://doi.org/10.1016/s0034-4257(96)00072-7

Gorelick, N., Hancher, M., Dixon, M., Ilyushchenko, S., Thau, D., Moore, R. (2017). Google Earth Engine: Planetary-scale geospatial analysis for everyone, Remote Sensing of Environment, 202, 18–27, ISSN 0034–4257, https://doi.org/10.1016/j.rse.2017.06.031

Goward, S. N., Huemmrich, K. F., & Waring, R. H. (1994). Visible-near infrared spectral reflectance of landscape components in western Oregon. *Remote Sensing of Environment*, *47*(2), 190–203. https://doi.org/10.1016/0034-4257(94)90155-4

Huemmrich, K. F., & Goward, S. N. (1997). Vegetation canopy PAR absorptance and NDVI: An assessment for ten tree species with the SAIL model. *Remote Sensing of Environment*, *61*(2), 254–269. https://doi.org/10.1016/S0034-4257(97)00042-4

Huete, A. R., Justice, C., Van Leeuwen, W. (1999). Modis vegetation index (MOD 13). Algorithm theoretical basis document version 3. University of Arizona ed., 1–120, https://modis.gsfc.nasa.gov/data/atbd/atbd_mod13.pdf

Khan, A., Khan, U., Waleed, M., Khan, A., Kamal, T., Marwat, S. N. K., Maqsood, M., & Aadil, F. (2018). Remote sensing: An automated methodology for olive tree detection and counting in satellite images. *IEEE Access*, *6*, 77816–77828. https://doi.org/10.1109/ACCESS.2018.2884199

Liknes, G. C., Perry, C. H., & Meneguzzo, D. M. (2010). Assessing tree cover in agricultural landscapes using high-resolution aerial imagery. Article 5 J. Terrest. Observ, 2(1), 38. https://www.srs.fs.usda.gov/pubs/34796

Malkoç, E., Rüetschi, M., Ginzler, C., & Waser, L. (2021). Countrywide mapping of trees outside forests based on remote sensing data in Switzerland. International Journal of Applied Earth Observation and Geoinformation, 100 (102336). ISSN 0303–2434, https://doi.org/10.1016/j.jag.2021.102336

Manning, A. D., Fischer, J., & Lindenmayer, D. B. (2006). Scattered trees are keystone structures – Implications for conservation. *Biological Conservation*, *132*(3), 311–321. https://doi.org/10.1016/j.biocon.2006.04.023

Meneguzzo, D., Liknes, G., & Nelson, M. (2013). Mapping trees outside forests using high-resolution aerial imagery: A comparison of pixel- and object-based classification approaches. *Environmental Monitoring and Assessment*, *185*(8), 6261–6275. https://doi.org/10.1007/s10661-012-3022-

Merot, P., Gascuel-Odoux, C., Walter, C., Zhang, X., & Molenat, J. (1999). Bocage landscape and surface water pathways. *Revue Internationale Des Sciences De l'Eau*, *12*(1), 23–44. https://doi.org/10.7202/705342ar

Mosquera-Losada, M.R., Santiago-Freijanes, J.J., Pisanelli, A. et al. (2018). Agroforestry in the European common agricultural policy. Agroforest Syst 92, 1117–1127. https://doi.org/10.1007/s10457-018-0251–5

Ottosen, T.B., Petch, G., Hanson, M., & Skjøth, C. A. (2020). Tree cover mapping based on Sentinel-2 images demonstrate high thematic accuracy in Europe. International Journal of Applied Earth Observation and Geoinformation, 84(101947). ISSN 0303–2434. https://doi.org/10.1016/j.jag.2019.101947

Paris, P., Camilli, F., Rosati, A., Mantino, A., Mezzalira, G., Dalla Valle, C., Franca, A., Seddaiu, G., Pisanelli, A., Lauteri, M., Brunori, A., Re, G. A., Sanna, F., Ragaglini, G., Mele, M., Ferrario, V., & Burgess, P. J. (2019). What is the future for agroforestry in Italy? *Agroforestry Systems*, *93*(6), 2243–2256. https://doi.org/10.1007/s10457-019-00346-y

QGIS Development Team (2018). *QGIS Geographic Information System*. Open Source Geospatial Foundation Project. http://qgis.osgeo.org

Rigueiro-Rodríguez, A., McAdam, J., & Mosquera-Losada, M. R. (eds). (2009). *Agroforestry in Europe: Current status and future prospects. Advances in agroforestry no* (Vol. 6, pp. 462). Berlin, Springer.

Rouse, J. W., Jr., Haas, R. H., Schell, J. A., & Deering, D. W. (1973). *Monitoring the vernal advancement and retrogradation (green wave effect) of natural vegetation*. (Vol. 93p). Prog. Rep. RSC 1978-1, Remote Sensing Center, Texas A&M Univ., College Station, . (NTIS No. E73-106393. . .

Santiago-Freijane, J. J., Pisanelli, A., Rois-Díaz, M., Aldrey-Vázquez, J. A., Rigueiro-Rodríguez, A., Pantera, A., Vityi, A., Lojka, A., Ferreiro-Domínguez, B., & Mosquera-Losada MR, N. (2018). Agroforestry development in Europe: Policy issues. *Land Use Policy*, *76*, 144–156. URL https://efi.int/publications/agroforestry-development-europe-policy-issues-2018-05-07

Saunders, D. A., Hobbs, R. J., & Margules, C. R. (1991). Biological consequences of ecosystem fragmentation: A review. *Conservation Biology*, *5*(1), 18–32. https://doi.org/10.1111/j.1523-1739.1991.tb00384.x

Schnell, S., Altrell, D., Ståhl, G., & Kleinn, C. (2015a). The contribution of trees outside forests to national tree biomass and carbon stocks – A comparative study across three continents. *Environmental Monitoring and Assessment*, *187*(1), 4197. https://doi.org/10.1007/s10661-014-4197-4

Schnell, S., Kleinn, C., & Ståhl, G. (2015b). Monitoring trees outside forests: A review. *Environmental Monitoring and Assessment*, *187*(9), 600. https://doi.org/10.1007/s10661-015-4817-7

Scott, D. W. (1979). On optimal and data-based histograms. *Biometrika*, *66*(3), 605–610. https://doi.org/10.1093/biomet/66.3.605

Shibu, J. (2009). Agroforestry for ecosystem services and environmental benefits: An overview. *Agroforestry Systems*, *76*(1), 1–10. https://doi.org/10.1007/s10457-009-9229-7

Singh, K., & Chand, P. (2012). Above-ground tree outside forest (TOF) phytomass and carbon estimation in the semi-arid region of southern Haryana: A synthesis approach of remote sensing and field data. *Journal of Earth System Science*, *121*(6), 1469–1482. https://doi.org/10.1007/s12040-012-0237-z

Tansey, K., Chambers, I., Anstee, A., Denniss, A., & Lamb, A. (2009). Object-Oriented classification of very high resolution airborne imagery for the extraction of hedgerows and field margin cover in agricultural areas. *Applied Geography*, *29*(2), 145–157. https://doi.org/10.1016/j.apgeog.2008.08.004

Vannier, C., & Hubert-Moy, L. (2014). Multiscale comparison of remote-sensing data for linear woody vegetation mapping. *International Journal of Remote Sensing*, *35*(21), 7376–7399. https://doi.org/10.1080/01431161.2014.968683

Wang, F., Huang, J., Tang, Y., & Wang, X. (2007). New vegetation index and its application in estimating leaf area index of rice. *Rice Science*, *14*(3), 195–203. https://doi.org/10.1016/s1672-6308(07)60027-4

Yang, C., Everitt, J. H., Bradford, J. M., & Murden, D. (2004). Airborne hyperspectral imagery and yield monitor data for mapping cotton yield variability. *Precision Agriculture*, *5*(5), 445–461. https://doi.org/10.1007/s11119-004-5319-8

Yang, J., Liu, C., & Zhang, L. (2010). Color space normalization: Enhancing the discriminating power of color spaces for face recognition. *Pattern Recognition*, *43*(4), 1454–1466. https://doi.org/10.1016/j.patcog.2009.11.014

Zomer, R. J., Neufeldt, H., Xu, J., Ahrends, A., Bossio, D., Trabucco, A., van Noordwijk, M., & Wang, M. (2016). Global tree cover and biomass carbon on agricultural land: The contribution of agroforestry to global and national carbon budgets. *Scientific Reports*, *6*(1), 29987. https://doi.org/10.1038/srep29987.